Reorganization of actin filaments by ADF/cofilin is involved in formation of microtubule structures during *Xenopus* oocyte maturation

Yuka Yamagishi and Hiroshi Abe
Department of Nanobiology, Graduate School of Advanced Integration Science, Chiba University, Chiba 263-8522, Japan

ABSTRACT We examined the reorganization of actin filaments and microtubules during *Xenopus* oocyte maturation. Surrounding the germinal vesicle (GV) in immature oocytes, the cytoplasmic actin filaments reorganized to accumulate beneath the vegetal side of the GV, where the microtubule-organizing center and transient microtubule array (MTOC-TMA) assembled, just before GV breakdown (GVBD). Immediately after GVBD, both *Xenopus* ADF/cofilin (XAC) and its phosphatase Slingshot (XSSH) accumulated into the nuclei and intranuclear actin filaments disassembled from the vegetal side with the shrinkage of the GV. As the MTOC-TMA developed well, cytoplasmic actin filaments were retained at the MTOC-TMA base region. Suppression of XAC dephosphorylation by anti-XSSH antibody injection inhibited both actin filament reorganization and proper formation and localization of both the MTOC-TMA and meiotic spindles. Stabilization of actin filaments by phalloidin also inhibited formation of the MTOC-TMA and disassembly of intranuclear actin filaments without affecting nuclear shrinkage. Nocodazole also caused the MTOC-TMA and the cytoplasmic actin filaments at its base region to disappear, which further impeded disassembly of intranuclear actin filaments from the vegetal side. XAC appears to reorganize cytoplasmic actin filaments required for precise assembly of the MTOC and, together with the MTOC-TMA, regulate the intranuclear actin filament disassembly essential for meiotic spindle formation.

INTRODUCTION

Oocyte maturation is defined by resumption of meiosis to release oocytes from arrest in meiotic prophase I. This process starts with the breakdown of the nuclear envelope of the germinal vesicle, a giant nucleus specifically formed in oocytes (i.e., germinal vesicle breakdown [GVBD] or nuclear envelope breakdown). In *Xenopus* oocytes, progesterone induces GVBD, with subsequent spindle formation and progression to metaphase II (Masui and Clark, 1979); formation of the white maturation spot (WMS) at the animal pole is a well-established indicator of GVBD. The yolk-free zone is formed at the vegetal region by releasing the nucleoplasm to the cytoplasm after GVBD. A disk-shaped organelle called the microtubule-organizing center and transient microtubule array (MTOC-TMA) assembles in the yolk-free zone to capture chromosomes in the cytoplasm and transport them to the animal cortex to form meiotic spindles (Jessus *et al.*, 1986; Gard, 1992). Thereafter, the MTOC-TMA disappears, and chromosomes are aligned on the spindle microtubules.

Actin filaments are well known for their significant roles in spindle migration and anchorage to the cortex in oocyte maturation processes in mouse oocytes (Field and Lénárt, 2011; Yi and Li, 2012; Li and Albertini, 2013; Almonacid *et al.*, 2014). In addition, actin and myosin also play major roles in spindle assembly during meiosis and mitosis (Weber *et al.*, 2004; Sandquist *et al.*, 2011). The actin filaments in *Xenopus* oocytes, which grow to a tremendous size (~1.2 mm in diameter) and possess a giant nucleus (the GV; 400–500 μm in diameter), localize in three cellular domains: the cortex, the nucleus,

and a network of cytoplasmic cables surrounding the GV (Loeder and Gard, 1994). The actin network that spans the entire nucleus appears to mechanically support the extremely large *Xenopus* oocyte nucleus, as shown by the action of exportin 6, a factor responsible for exclusion of actin from nuclei in somatic cells: injection of exportin 6 into nuclei causes actin filaments to disappear and thereby increases the fragility of these nuclei (Bohnsack *et al.*, 2006). In their pioneering work, Gard *et al.* (1995) demonstrated that during oocyte maturation, the normal organization of the MTOC-TMA complex and meiotic spindle anchorage to the cortex are disrupted when actin filament formation is inhibited by cytochalasin B. We further demonstrated that microinjection of phalloidin (an F-actin–stabilizing drug) into *Xenopus* oocytes prevents GVBD and leads to an unusual formation of microtubules in both the nuclei and cytoplasm during oocyte maturation (Okada *et al.*, 2012).

Many actin-binding proteins are involved in the regulation of the intracellular dynamics of actin filaments. The ADF/cofilin family of proteins is essential for severing and depolymerizing actin filaments to increase the rate of actin filament turnover (Ono, 2007; Van Troys *et al.*, 2008; Bernstein and Bamburg, 2010). ADF/cofilin is inactivated and reactivated via phosphorylation/dephosphorylation by LIM kinase (Limk; Arber *et al.*, 1998; Yang *et al.*, 1998) and Slingshot (SSH; Niwa *et al.*, 2002), respectively. The formation of WMS and the MTOC-TMA can be disrupted by injection of constitutively active Limk in *Xenopus* oocytes; this disruption by Limk can be suppressed when combined with a constitutively active form of *Xenopus* ADF/cofilin (XAC; Abe *et al.*, 1996; Takahashi *et al.*, 2001). Taken together, the dynamic regulation of actin filaments by ADF/cofilin appears to be essential for the proper formation of microtubule structures, including the MTOC-TMA. In fact, we already showed the role of *Xenopus* Slingshot (XSSH) in the formation of microtubule structures during oocyte maturation (Iwase *et al.*, 2013).

SSH was originally identified as an ADF/cofilin-specific phosphatase in *Drosophila* and humans (Niwa *et al.*, 2002). This protein colocalizes with actin filaments in cultured cells, and its association with actin filaments markedly enhances phosphatase activity (Nagata-Ohashi *et al.*, 2004). Phosphorylation of the SSH C-terminal domain (the tail domain) prevents its binding to actin filaments by association of the 14-3-3 proteins at the phosphorylation site (Nagata-Ohashi *et al.*, 2004; Soosairajah *et al.*, 2005). XSSH is also phosphorylated and activated by binding to actin filaments (Tanaka *et al.*, 2005a,b). In contrast to the action of SSH in mammalian cells, phosphorylation of XSSH at multiple sites within the tail domain occurs immediately after GVBD and is accompanied by dephosphorylation of XAC, which is mostly phosphorylated in immature oocytes (Iwase *et al.*, 2013). Injection of the anti-XSSH antibody, which blocks full phosphorylation of XSSH after GVBD, caused inhibition of both meiotic spindle formation and XAC dephosphorylation (Iwase *et al.*, 2013); this inhibitory effect is suppressed by coinjection of the antibody and constitutively active XAC. Thus elevation of actin dynamics by XAC activation through XSSH phosphorylation appears to be essential for the meiotic spindle assembly in *Xenopus laevis*.

In this study, we investigate the structure of intranuclear and cytoplasmic actin filaments and the regulatory roles of XAC and XSSH in actin filament dynamics for proper assembly of the MTOC-TMA and meiotic spindles during oocyte maturation in *X. laevis*.

RESULTS

Characterization of intranuclear actin filaments during oocyte maturation before GVBD

We first observed the morphology of intranuclear actin filaments during oocyte maturation. Because oocytes indeed possess a high background of fluorescence by immunofluorescence microscopy, we confirmed that control staining by each secondary antibody alone did not stain any structures that were stained specifically by the primary antibody or tetramethylrhodamine (TMR)-phalloidin (Supplemental Figure S1). The mesh of intranuclear actin filaments was clearly stained with Alexa 488–phalloidin in vertical sections of immature stage VI oocytes (Figure 1, A–C). Actin filaments were also located in the cytoplasm surrounding the nuclei (Figure 1A, arrows), as expected (Loeder and Gard, 1994). We confirmed that these filaments are present outside the nuclei by dual staining with anti-lamin antibody and Alexa 488–phalloidin (Figure 1B). Magnification of intranuclear actin filament networks in vertical sections (Figure 1C) revealed the transition of the network structures along the animal-to-vegetal axis. The actin networks were dense and sponge-like at the vegetal side of the nuclei (Figure 1D), as previously reported (Bohnsack *et al.*, 2006), and rather loose and straight toward the animal pole (Figure 1E). We confirmed these structural differences by quantifying the mesh size (Figure 1F). Furthermore, the amount of intranuclear actin filaments fluctuated during oocyte maturation until GVBD (Supplemental Figure S2A); the intensity of actin filament staining increased at the relative time point of 0.2 (about one-fifth of the way between progesterone treatment and GVBD) and returned to its original level at relative time points 0.4 and 0.6 (Supplemental Figure S2A).

Next, using cytoplasmic *Xenopus* Cap1/Srv2 (XCap1) as a reference protein that persists during maturation, we quantified the change in fluorescence intensity of intranuclear actin filaments (Supplemental Figure S2B). XCap1 was confirmed to be present in the cytoplasm, as judged by immunoblotting (Supplemental Figure S2B) and immunofluorescence microscopy (Supplemental Figure S2C). The relative intensity of intranuclear actin filaments increased specifically at a relative time point between 0.2 and 0.4 (Supplemental Figure S2D), which corresponds to the increase in the amount of precipitated actin specifically between the relative time points of 0.1 and 0.3 on the F-actin sedimentation assay of isolated nuclei (Supplemental Figure S3, A and B). These isolated nuclei, which were immediately frozen and double stained with anti-lamin antibody and Alexa 488–phalloidin, showed limited staining outside the nuclei by Alexa 488–phalloidin (Supplemental Figure S3C), reflecting changes in the amount of intranuclear actin filaments before GVBD.

Reorganization of actin filaments and microtubules during oocyte maturation

We monitored the progression of GVBD by lamin staining. Figure 2A shows clear staining of lamin filaments underlying the nuclear envelopes in immature oocytes; there was relatively smooth staining at the animal side and wavy staining at the vegetal side. As maturation progressed, nuclear envelopes on both sides became much wavier (Figure 2B), and GVBD occurred initially at the vegetal surface of the nuclei (Figure 2C). Of note, the nuclear volume shrank and the yolk-free region expanded according to the progression of oocyte maturation immediately after GVBD. In immature oocytes, cytoplasmic actin filaments appeared to surround the nuclei (Figures 1A and 2A). At the relative time point of 0.8 (immediately before GVBD), cytoplasmic actin filaments were reorganized and assembled into a line just beneath the vegetal side of the nuclei, where the yolk-free zone was formed (Figure 2B, arrow). Of interest, at the same relative time point, cytoplasmic yolk granules appeared to associate tightly with the isolated nuclei, whereas the cytoplasmic actin filaments at the base of the nuclei were scarcely visible (Supplemental Figure S3C). We also found that the cytoplasmic actin assembly at the base of the
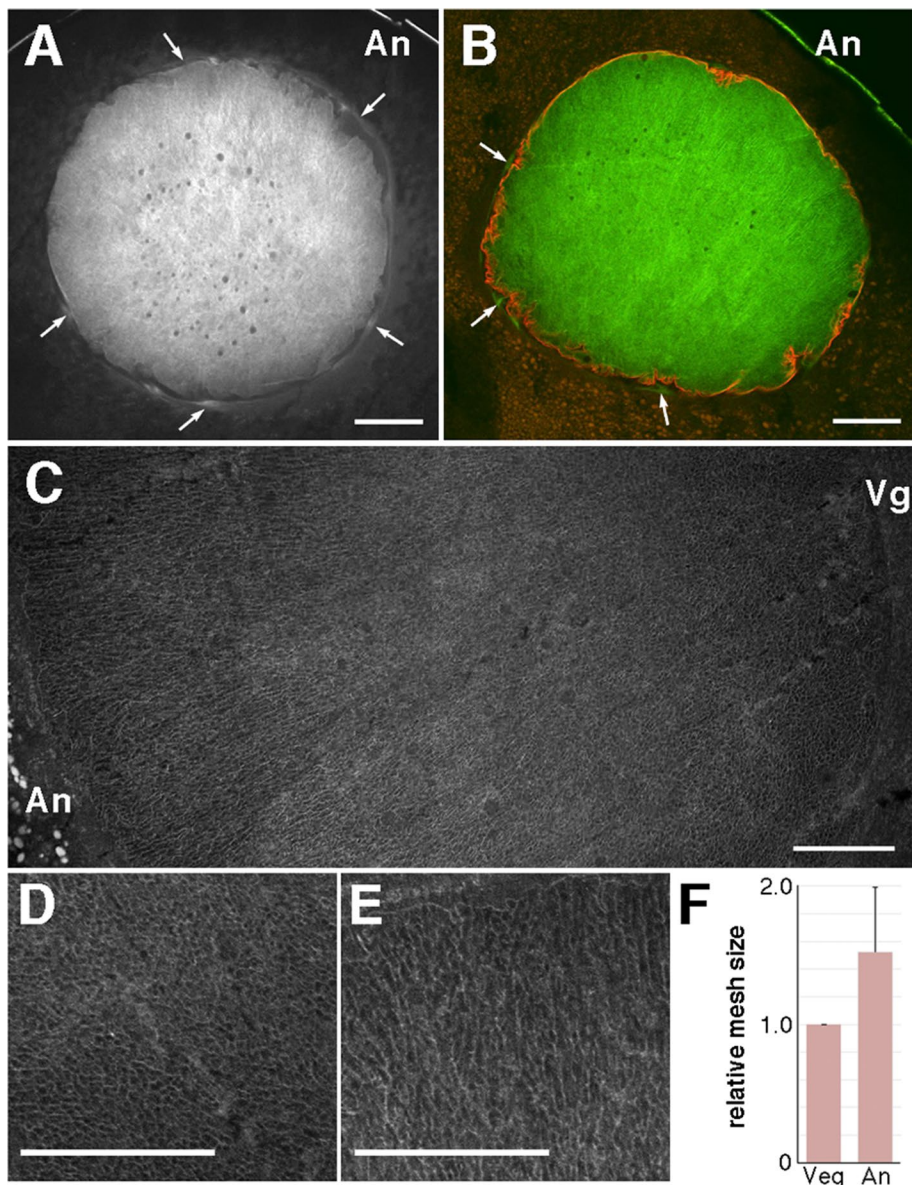
FIGURE 1: Structure of the intranuclear actin filaments. Eleven oocytes derived from four different females were examined. The nucleus of a midsagittal (animal–vegetal) cryosection of a full-grown stage VI oocyte was stained with Alexa 488–phalloidin (A) and double stained with Alexa 488–phalloidin and anti-lamin antibody (B). Arrows indicate the actin filaments surrounding the nucleus. (C) Enlarged image of the nucleus by assembling three shots, which had to be taken to cover one section, in a composite plate. The vegetal region (D) and animal region (E) are further enlarged. (F) Comparison of the actin filament mesh size between the vegetal (Veg) and animal (An) sides. The area of the space surrounded by actin filaments (the mesh hole) was measured over a set range by ImageJ software. Twelve oocytes from nine different females were measured. Relative mesh size at the animal side. Bars, 100 µm (A, B), 50 µm (C–E). An, animal pole; Vg, vegetal pole.

lamin filaments formed vesicle-like structures in the yolk-free region after GVBD (Figure 2, D–H)

Microtubules showed circumferential distribution around the nuclei of immature oocytes (Figure 3A). Of note, at the relative time point of 0.8, microtubules colocalized with the lined actin filaments formed in the cytoplasm beneath the vegetal side of the nuclei as mentioned earlier (Figure 3B, arrows) and then formed the MTOC-TMA (Figure 3C). After GVBD immediately after formation of the MTOC-TMA, the cytoplasmic actin filaments were present at the base of the MTOC-TMA and the intranuclear actin filaments disassembled from the vegetal region, into which the TMA elongated from the MTOC (Figure 3C). However, the microtubules did not enter the animal region, where the residual intranuclear actin filaments were still present. When the residual intranuclear actin filaments disappeared, the MTOC-TMA migrated to the animal side and retained the actin filaments at its base (Figure 3D).

XAC and XSSH participate in reorganization of actin filaments in nuclei

To monitor the actin filament dynamics in the nuclei, we examined the amount and phosphorylation state of intranuclear XAC in isolated nuclei, as XAC is a key regulator for actin dynamics. Both XAC and actin significantly accumulated in the nuclei (Supplemental Figure S4A). We previously showed that XAC is highly phosphorylated in stage VI oocytes (Iwase et al., 2013). XAC in isolated nuclei was also phosphorylated, and its phosphorylation balance gradually shifted toward dephosphorylation until GVBD, although cytoplasmic XAC was highly phosphorylated, and its significant dephosphorylation occurred from GVBD (Supplemental Figure S4B). On the other hand, XSSH, the XAC activator, was also present in the nuclei, but its amount was much smaller than that of XAC (Supplemental Figure S4A). This intranuclear XSSH exhibited a slight mobility shift on SDS–PAGE (Supplemental Figure S4A, arrow), indicating that the intranuclear XSSH is partially phosphorylated. Therefore intranuclear actin filaments can be regulated by XAC via its phosphorylation control.

Localization of XAC and XSSH in oocytes

We observed the localization of XAC and XSSH in oocytes during maturation. As shown in Figure 4, A and B, both XAC and XSSH diffused in the cytoplasm, with XAC being more evident in the nuclei of immature oocytes. We again confirmed that the XAC and XSSH stains are positive, because of the drastic decrease in the fluorescence intensity of sections treated with the secondary antibody

nucleus at the relative time point of 0.8 was scarcely observed when oocytes were gently fixed by paraformaldehyde at room temperature without quick-freezing by liquid nitrogen (unpublished data). Therefore cytoplasmic actin filament assembly may be highly dynamic and not be stable enough to endure the isolation process and gentle fixation. The intranuclear actin filaments, despite the decrease in staining intensity, were retained after GVBD when lamin filaments disassembled to crowd downward to the vegetal side (Figure 2C). The cytoplasmic actin filaments at the base of the MTOC remained localized at the vegetal side (Figure 2C, arrow). The disassembled
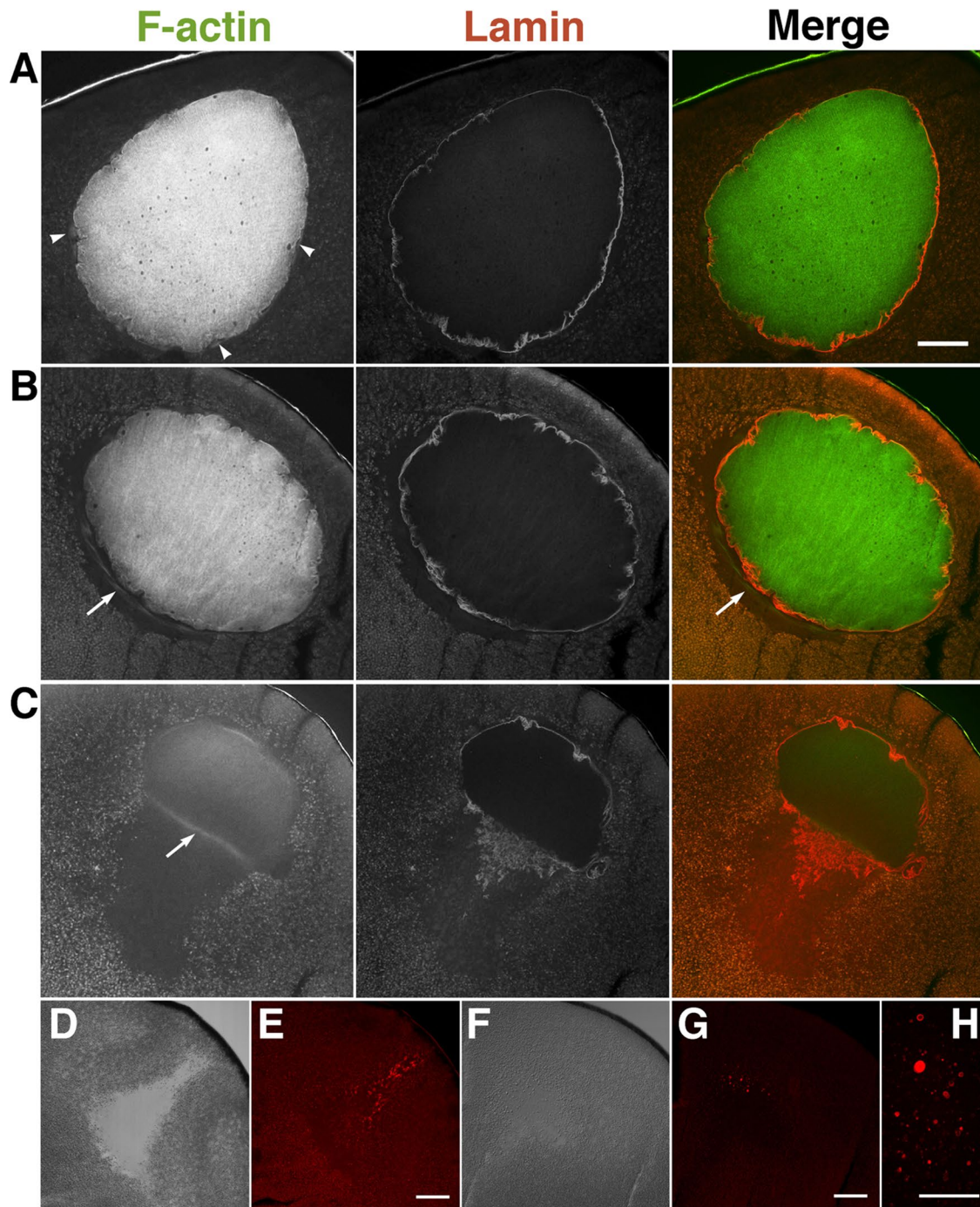
FIGURE 2: Staining of actin filaments and lamin during oocyte maturation. Representative confocal microscopy images of midsagittal sections of oocytes pretreated with progesterone (A), at the relative time point of 0.8 (just before GVBD; B), and just after GVBD (C) were double stained with Alexa 488–phalloidin (F-actin) and anti-lamin antibody (lamin). Nine oocytes from three different females were examined. Arrows indicate the cytoplasmic actin filaments surrounding the nucleus. Differential interference contrast (DIC; D, F) and lamin-staining images (E, G, H) of maturing oocytes at WMS formation (the relative time point of 1.0; D, E) and 2 h after WMS formation (F–H). Bars, 100 μm (A, E, G), 50 μm (H).

alone (Figure 4C). After GVBD, the staining intensity of both XAC and XSSH markedly increased in the nuclei (Figure 4, D and G, asterisks), whereas they were exclusively absent from the base region of the MTOC-TMA (Figure 4, D–I, arrows). These exclusive distributions of the respective proteins at the base of the MTOC-TMA were retained when the MTOC-TMA further developed (Figure 4, J–M), suggesting that the actin filaments can be protected at the base

region of the MTOC-TMA from disassembly by XAC. Somewhat distinct staining patterns were observed in the nuclei by analyzing the fluorescence intensity of both XSSH (Figure 4F) and XAC (Figure 4I) from the animal to the vegetal direction at the center of the nuclear region; XSSH appeared to be relatively uniformly staining at the center region of nuclei where the TMA is sparse, whereas XAC appeared to increase toward the animal region.
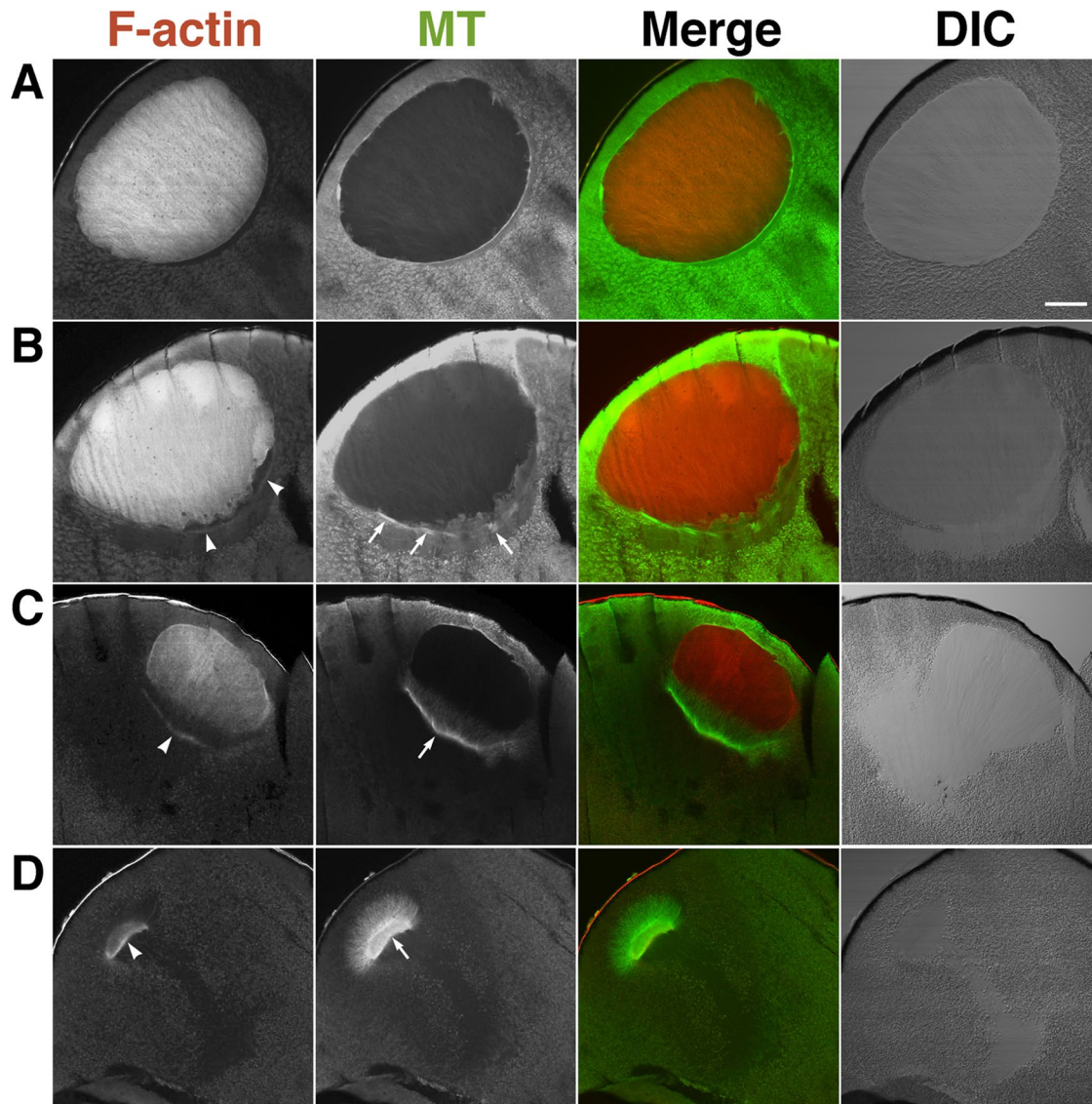
FIGURE 3: Staining of actin filaments and microtubules during oocyte maturation. Nine oocytes from three different females were examined. Midsagittal sections of oocytes pretreated with progesterone (A), at the relative time point of 0.8 (just before GVBD; B), just after GVBD (C), and at the relative time point of 1.0 (D) were double stained with TMR–phalloidin (F-actin) and anti-tubulin antibody (MT). Merged and DIC images are also shown. Arrowheads indicate the cytoplasmic actin filament bundles. Arrows in B and in C and D indicate microtubule bundles and the MTOC-TMA, respectively. Bar, 100 μm.

Injection of XSSH antibodies suppresses actin filament reorganization and MTOC-TMA formation

We previously demonstrated that the injection of anti-XSSH antibody inhibits XAC dephosphorylation and MTOC-TMA formation (Iwase et al., 2013). In this study, we injected a 1:1 mixture of the purified anti-XSSH immunoglobulin G (IgG) and anti-XSSH IgG conjugated with a nuclear localization signal nonapeptide (NLS-peptide) in order to strengthen the inhibition of the intranuclear XSSH activity. Supplemental Figure S5A shows that NLS-peptide–conjugated anti-XSSH IgG was successfully introduced into the nuclei. We confirmed that this antibody injection also inhibits WMS formation, as well as anti-XSSH IgG injection (Supplemental Figure S5B). In addition, we confirmed that the effect of anti-XSSH antibody injection is specific, since injection of the purified IgG, which specifically binds to avian and mammalian cofilin but not to XAC (designated as MAB-22; Abe et al.,

1989) did not affect the process of oocyte maturation even when the NLS-peptide was conjugated (Supplemental Figure S5B). As we previously showed (Iwase et al., 2013), when oocytes were homogenized in phosphate-buffered saline (PBS) and centrifuged, the amount of XSSH in the supernatant decreased in anti-XSSH IgG-NLS–injected oocytes (Supplemental Figure S5C). In addition, the XSSH bands in anti-XSSH IgG-NLS–injected oocytes were also situated at the midway between the band in immature oocytes (nonphosphorylated XSSH) and that in control (matured) oocytes (hyperphosphorylated XSSH). These results taken together show that anti-XSSH IgG-NLS retains the same activity as the original anti-XSSH IgG.

In immature oocytes injected with antibody, the cytoplasmic staining slightly increased (Supplemental Figure S6, A and B) and the intranuclear actin mesh formed an obscure structure (Supplemental Figure S6, C and D). As maturation progressed, cytoplasmic
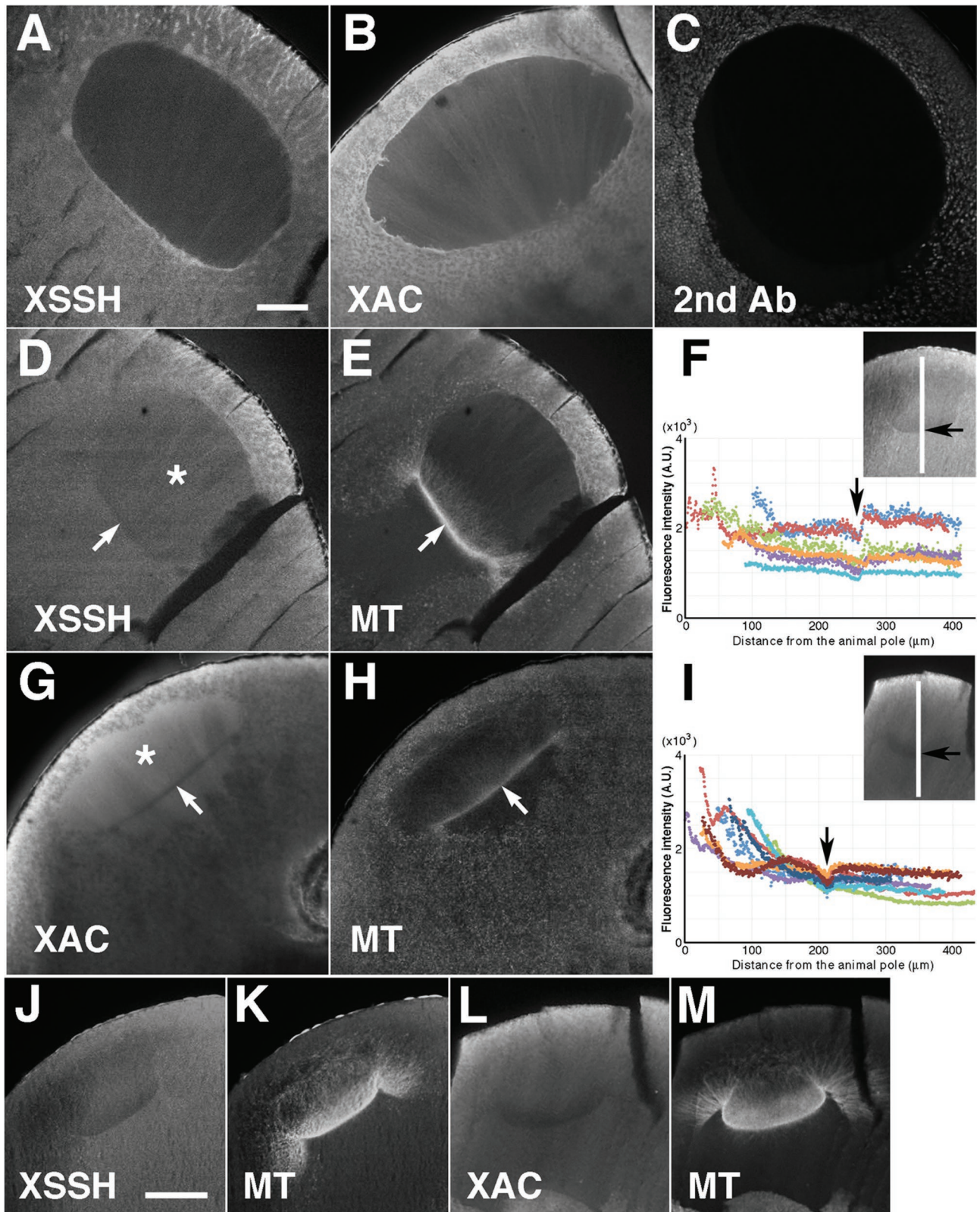
FIGURE 4: Localization of XSSH and XAC during oocyte maturation. Midsagittal sections of full-grown oocytes (A, B) were stained with anti-XSSH antibody (A) and anti-XAC antibody (B). For the negative control, the cryosection of the oocyte at the relative time point of 0.8 was stained with Alexa 488–labeled secondary antibody against rabbit IgG alone (C). Midsagittal sections of maturing oocytes just after GVBD (D–I) and at the relative time point of 1.0 (J–M) were double stained with anti-XSSH antibody (D, J) and anti-tubulin antibody (E, K) or with anti-XAC antibody (G, L) and anti-tubulin antibody (H, M). At the relative time point of 1.0 (at the same time point as in J and L), the fluorescence intensity of either XSSH (F) or XAC (I) staining from the animal to the vegetal direction at the center of the nuclear
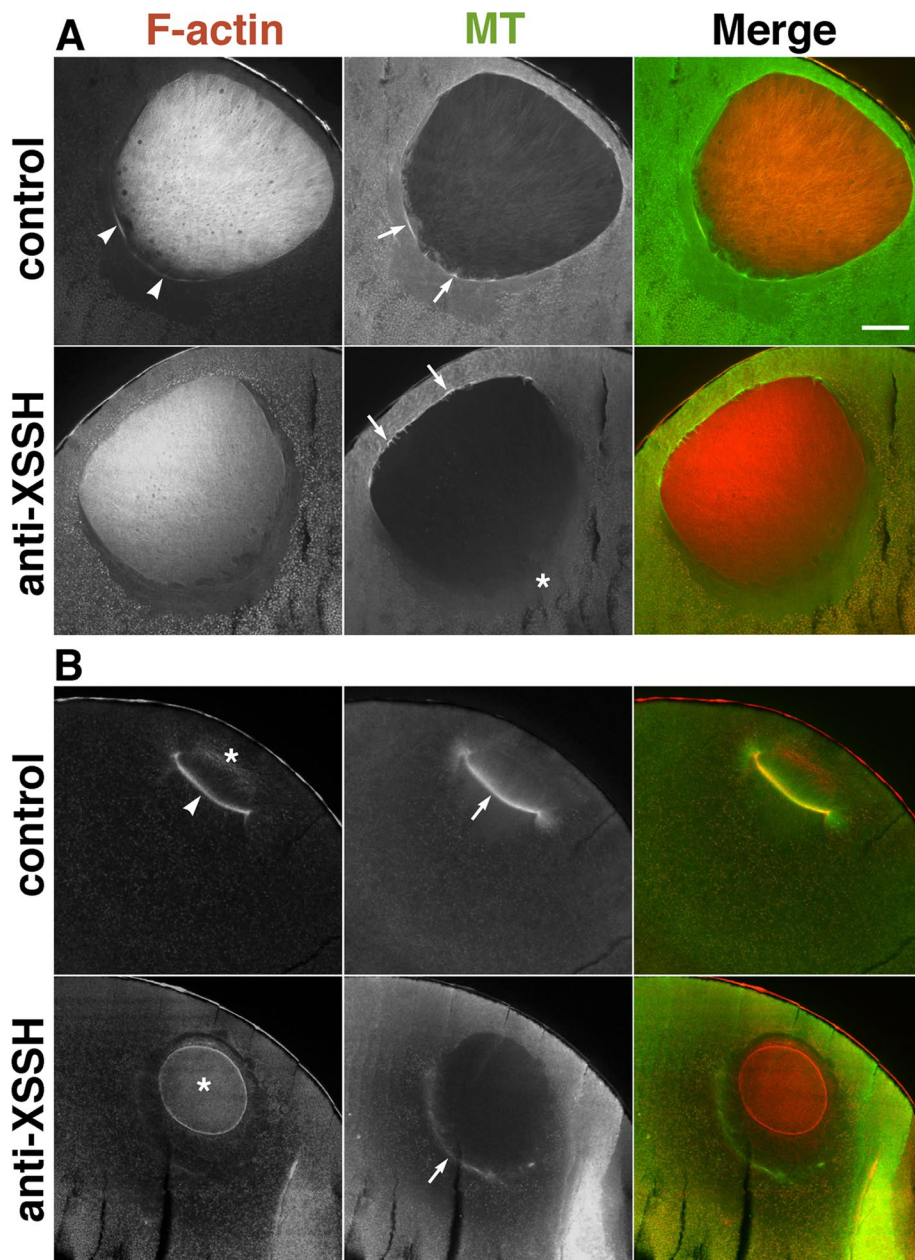
FIGURE 5: Effects of injection of anti-XSSH antibody on assembly of the MTOC-TMA. Midsagittal sections of oocytes just before (A) or after (B) GVBD, injected with buffer alone (control) or with 10 mg/ml of 1:1 mixture of anti-XSSH IgG and anti-XSSH IgG-NLS (anti-XSSH), were double stained with TMR–phalloidin (F-actin) and anti-tubulin antibody (MT). (A) Assembly of the cytoplasmic actin filaments (arrowheads) and microtubule bundles (arrows) at the basal region of nuclei is clearly visible in the control but faint at the basal region of nuclei in antibody-injected oocytes (asterisk). On the other hand, microtubule bundles are evident at the animal side of the nuclei of antibody-injected oocytes. (B) The cytoplasmic actin filaments (arrowhead) are apparent at the base of the MTOC-TMA (arrow) in the control, whereas the intranuclear actin filaments (asterisks) clearly remained in a globular shape and the MTOC-TMA is faint at the basal region of the nuclei in antibody-injected oocytes. Merged images are also shown. Bar, 100 μm. Images in A and B are representative staining of 11 and 17 oocytes from five females, respectively.

actin filaments were no longer aligned beneath the vegetal side of the nuclei immediately before GVBD (Figure 5A), and microtubules did not assemble there (Figure 5A, asterisk); we previously demonstrated this mislocalization of microtubules by anti-XSSH antibody injection (Iwase *et al.*, 2013). These results suggest that assembly of actin filaments beneath the vegetal side of the nuclei is required for the concentration of the MTOC to the same region. After GVBD, when control oocytes formed the MTOC-TMA that elongated into the nuclear region, the antibody-injected oocytes retained the intranuclear actin filaments as shrunken globular clusters of nuclear remnants (Figures 5B and 6H), indicating that the unidirectional disassembly of intranuclear actin filaments from the vegetal side was indeed inhibited. We could not confirm the presence or absence of lamin filaments in those nuclear remnants because of the cross-reactivity of secondary antibody for anti-lamin antibody and injected anti-XSSH antibody. In antibody-injected oocytes, faint staining of the cytoplasmic actin filaments was barely visible at the basal region of the nuclei compared to marked staining in control oocytes (Figure 5B, arrowhead). Furthermore, instead of developing MTOC-TMA, frail microtubule structures were colocalized with the faint cytoplasmic actin filaments without elongating the microtubule array into the globular actin filament structures (Figure 5B, arrows). These observations were consistent in antibody-injected oocytes, which did not form WMS when the control oocytes passed the relative time point of 1.0 (Supplemental Figure S5D); three additional examples are shown in Supplemental Figure S7A. Finally, the nuclear remnants of actin filaments disappeared in the antibody-injected oocytes (Supplemental Figure S7A, middle).

Because the antibody suppresses XAC dephosphorylation in oocytes, the dynamic state of actin filaments might shift to a stabilized state in antibody-injected oocytes. Thus we examined the effects of phalloidin on the formation of the MTOC-TMA and intranuclear actin filaments. As shown in Figure 6, A–D, when phalloidin was injected into immature oocytes, the nuclei slightly shrank to form the yolk-free region (Figure 6, B and D). Actin filaments surrounding nuclei with the yolk-free region were evident (Figure 6D,

region (shown with the white line in insets) was examined in different oocytes (six for XSSH and eight for XAC) using ImageJ software. The abscissa of the graphs is the number of pixels from the animal side, and the ordinate represents the fluorescence intensity (arbitrary units). Arrows indicate position of the base of the MTOC-TMA. The asterisks (D, G) indicate the nuclear region. Bars, 100 μm. Images are representative staining from at least 12 oocytes from four different females.
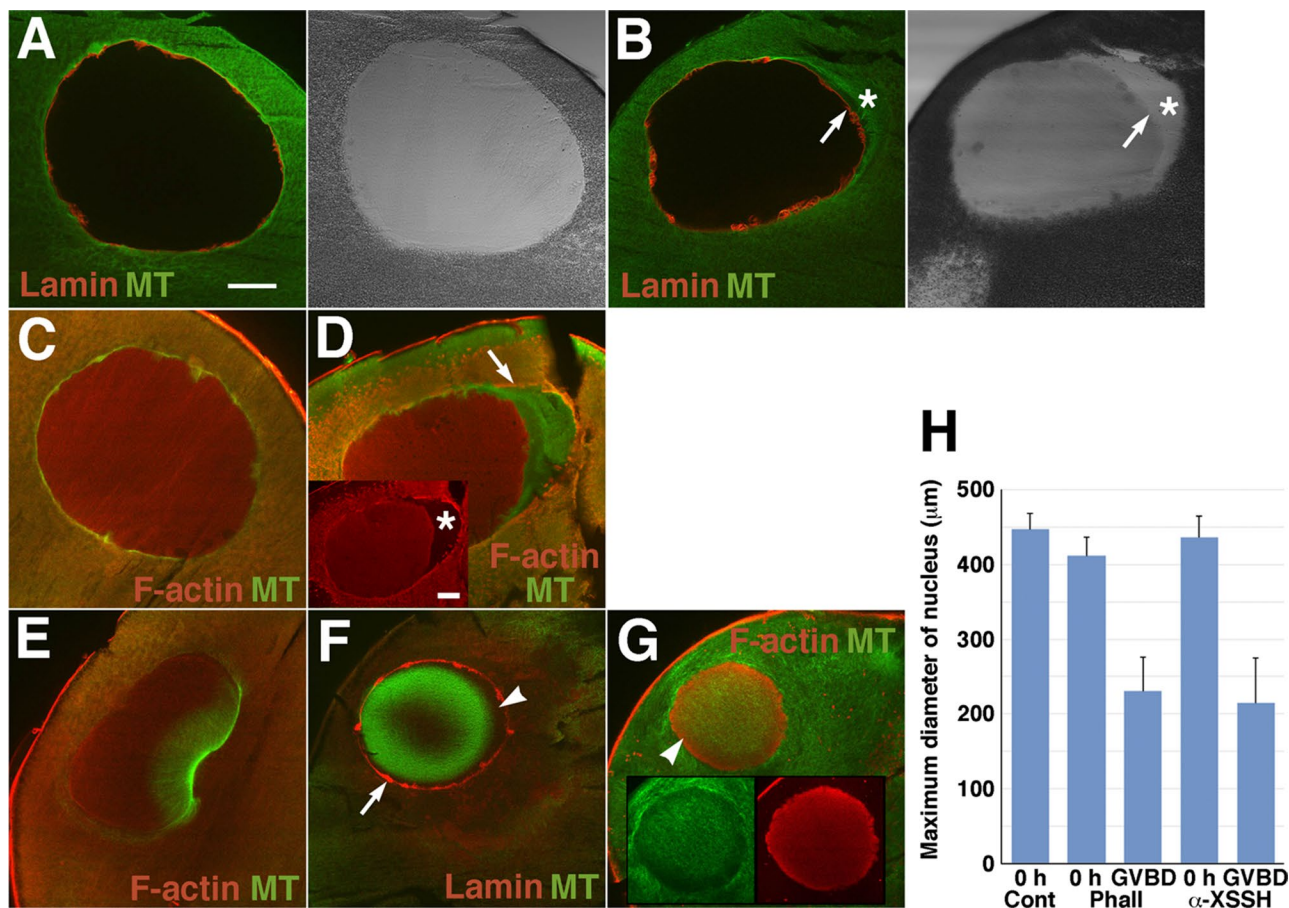
FIGURE 6: Effects of phalloidin injection on intranuclear actin filaments and assembly of the MTOC-TMA. Midsagittal sections of immature oocytes (A–D) and oocytes after GVBD (E–G), injected with vehicle alone (control; A, C, E) or with 10 mM phalloidin (B, D, F, G), were double stained with anti-lamin (red) and anti-tubulin (green) antibodies (A, B, F) or anti-actin (red) and anti-tubulin (green) antibodies (C– E and G). Merged images and DIC images are shown. Inset in D, anti-actin staining alone. Insets in G, images stained by anti-tubulin (green) and anti-actin (red) antibodies. Arrows in B and F indicate the nuclear periphery stained by anti-lamin antibody. Asterisks in B and D indicate the yolk-free region. Arrow in D represents the cytoplasmic actin filaments surrounding the nucleus. Arrowhead in F indicates the unstained space where actin filaments might be present as shown by the arrowhead in G. (H) Maximum diameter of the nuclei of oocytes injected with vehicle alone (Cont, $n = 6$), 10 mM phalloidin (Phall; 0 h, $n = 4$; GVBD, $n = 11$), or anti-XSSH antibody (α-XSSH; 0 h, $n = 4$; GVBD, $n = 5$) before progesterone treatment (0 h) or at GVBD. The gross area was measured from each section (the section that had maximum area of nuclei was selected from serial sections) by ImageJ software, and the maximum diameter was calculated as a perfect circle.
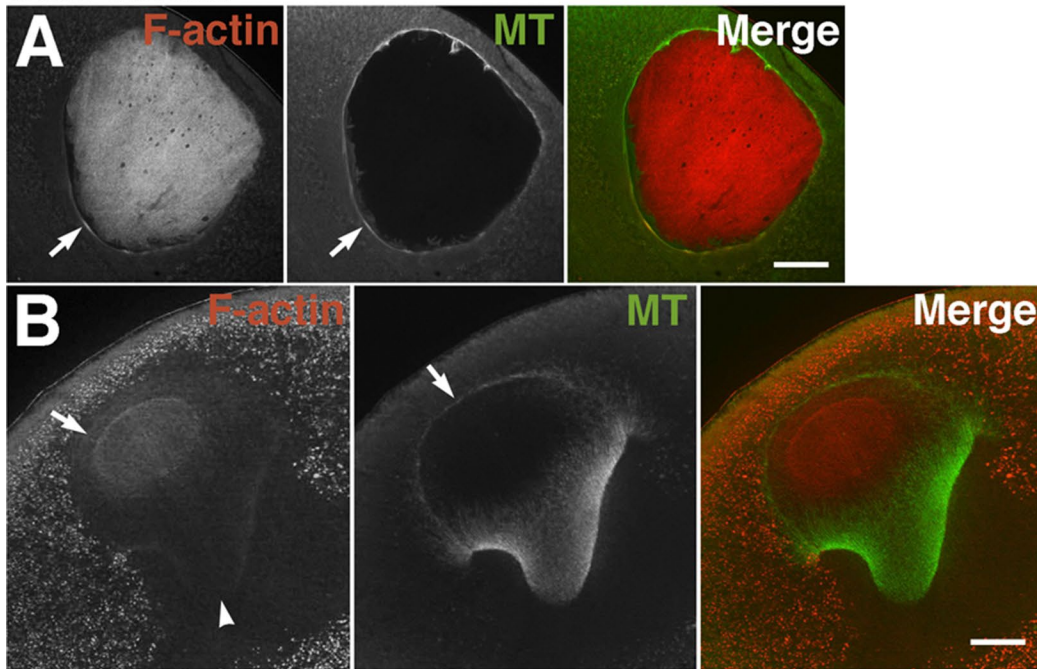
arrow). When control oocytes reached GVBD (Figure 6E), the nuclei of phalloidin-injected oocytes significantly shrank to show globular shapes with increasing staining of intranuclear actin filaments (Figure 6, F–H), suggesting that disassembly of the mesh structure, rather than depolymerization of actin filaments, is predominant during this process. Phalloidin-injected oocytes formed neither cytoplasmic actin filaments at the vegetal side beneath the nuclei nor the MTOC-TMA. Treating oocytes with jasplakinolide showed the similar results—shrinkage of nuclei, lack of accumulation of actin filaments at the vegetal side of nuclei, and a defect of MTOC-TMA formation (Supplemental Figure S8).

Nuclear lamin staining was retained in phalloidin-injected oocytes treated with progesterone (Figure 6F), most likely because the envelopes had become permeable since microtubules had localized in the nuclei. The complementary staining pattern of actin filaments and microtubules was characteristic of the nuclei of phalloidin- or jasplakinolide-treated oocytes; actin filaments surrounded the microtubules located at the central region of nucleoplasm

(Figure 6, F and G, and Supplemental Figure S8D; partly reported by Okada et al., 2012). In particular, jasplakinolide-treated oocytes showed strong actin filament staining at the circumferential nucleoplasm of the nuclear remnant. When control oocytes reached metaphase I, actin staining disappeared only at the vegetal side of nuclear remnants, and microtubule arrays developed in and around the remnants (Supplemental Figure S8D).

Next, to counteract the antibody injection, we injected constitutively active chick S3A cofilin into oocytes in order to increase actin dynamics (thereby preventing proper regulation). Using MAB-22, we could easily confirm introduction of chick cofilin into oocytes by either immunoblotting or immunofluorescence microscopy. Immediately before GVBD, the localization of actin filaments and microtubules in injected oocytes seemed to be the same as in normal oocytes (Figure 7A; compare with Figures 3B and 5A, control). However, an atypically curved and split MTOC-TMA was formed immediately after GVBD (Figure 7B). Although the TMA was well developed, actin staining appeared to be less evident, especially at the
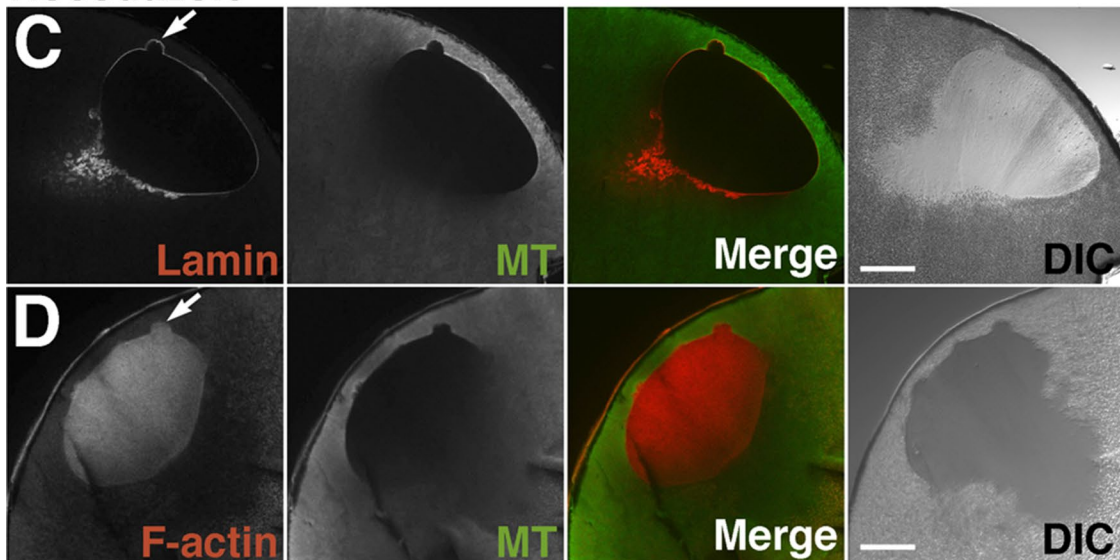
FIGURE 7: Effects of injection of 2.5 mg/ml chick S3A-cofilin (A, B) and treatment of 20 µg/ml nocodazole (C, D) on disassembly of intranuclear actin filaments and assembly of the MTOC-TMA. Midsagittal sections of S3A-cofilin–injected oocytes immediately before (A) or immediately after (B) GVBD were double stained with TMR-phalloidin (F-actin) and anti-tubulin antibody (MT). (A) Assembly of the cytoplasmic actin filaments and microtubule bundles (arrows) at the basal region of the nuclei is clearly visible in S3A-cofilin–injected oocytes. Twelve oocytes from six different females were examined. (B) Assembly of the MTOC-TMA is affected by S3A-cofilin injection. The TMA itself is well developed, but actin staining disappears from the base of the split region of the MTOC-TMA (arrowhead). Atypical microtubule structures have formed at the animal side as they surround the nuclear region (arrows). A faint staining of actin filaments (indicated by arrow in the F-actin panel) is also visible around the animal side of the residual nuclear actin filaments. Six oocytes from three different females were examined. Midsagittal sections of 20 µg/ml nocodazole–treated oocytes immediately after GVBD were double stained with anti-lamin and anti-tubulin antibodies (C) or TMR-phalloidin and anti-tubulin antibody (D). Merged and DIC images are also shown. Arrows indicate bleb-like protrusions characteristic of nocodazole-treated oocyte nuclei. Disassembly of the intranuclear actin filaments from the vegetal side is retarded. Twelve oocytes from three different females were examined.

base of the split MTOC-TMA (Figure 7B, arrowhead). In addition, microtubules formed unusual structures at the animal side as they surround the nuclear region; faint staining of actin filaments was also visible in this region. These observations were consistently reproduced, and three additional examples are shown in Supplemental Figure S7B. Each TMA of the S3A cofilin-injected oocytes developed and elongated much more than that of control oocytes. The residual intranuclear actin filaments disappeared more rapidly than those of control oocytes. These results suggest that overactivity of ADF/cofilin disassembles the actin filaments at the base of the MTOC-TMA to inhibit its precise formation.

To address whether retention of actin filaments at the base of MTOC-TMA also depends on the assembly of microtubules, we treated maturing oocytes at the relative time point of 0.5 with nocodazole; the efficacy of this drug is easily discriminated by the absence of WMS formation. As shown in Figure 7, C and D, both the MTOC-TMA and actin filaments were absent at the vegetal side beneath the nucleus of nocodazole-treated oocytes, whereas the control oocytes developed the MTOC-TMA. Of note, disassembly of intranuclear actin filaments from the vegetal side appeared to be retarded, although lamin was disassembled from the vegetal side of the nuclei. The retardation of disassembly of intranuclear actin filaments was mostly observed in nocodazole-treated oocytes fixed at the relative time point of 1.0 for control oocytes. In addition, bleb-like protrusions from the relatively smooth nuclear surface, as judged by the lamin staining, were characteristic in the nocodazole-treated oocytes undergoing GVBD (Figure 7, C and D, arrows). From these observations, it is likely that cytoplasmic actin filaments and microtubules cooperate in forming the MTOC-TMA. Moreover, unidirectional disassembly of intranuclear actin filaments from the vegetal side may require correct formation of MTOC-TMA.

Given that antibody injection suppresses the formation of MTOC-TMA, meiotic spindle assembly may also be affected. In fact, compared to control oocytes, which formed metaphase I spindles at the animal cortices (Figure 8A, showing the prometaphase I spindle), antibody-injected oocytes showed malformation of the metaphase I spindle with disrupted microtubule bundles around the chromosomes (Figure 8B). We could not show here any metaphase I spindles that oriented vertically to the cortex, whereas metaphase II spindles were easily observed in the serial sections of the control oocytes (Figure 8, C–E). Although metaphase II spindles in the antibody-injected oocytes often showed aberrant or barrel-like shapes at the cortex (Figure 8F), spindles that seemed to align chromosomes well at the equatorial plane sometimes formed at the center of the antibody-injected oocytes without anchoring to the cortex (Figure 8, G and H). On the other hand, in S3A-cofilin–injected oocytes, the metaphase I spindles mostly localized in the yolk-free region without anchoring to the cortex (Figure 8J; three examples are shown). We could observe malformed metaphase I spindles—for example, the spindle of chromosomes scattered around the yolk-free region, not integrated into the spindle microtubules—but changes in the shape of spindles could not be distinguished exactly between the control (Figure 8I) and S3A-cofilin injection. This problem mainly stems from the difficulty in encountering the metaphase I spindle just oriented vertically to the oocyte cortex. On the other hand, metaphase II spindles seemed to appear at the cortex without any defects in shape in S3A-cofilin–injected oocytes (unpublished data), although the detailed structure could not be examined in sections.

DISCUSSION

In this study, we showed dynamic organization of cytoplasmic and intranuclear actin filaments and formation of microtubule structures

during oocyte maturation. We previously demonstrated that injection of anti-XSSH antibody inhibits spindle assembly (Iwase et al., 2013), although the precise effect of antibody injection on cellular actin organization was unclear. Here we confirmed by immunofluorescence microscopy that anti-XSSH antibody injection actually stabilizes both cytoplasmic and intranuclear actin filaments to suppress their reorganization, which should originally occur during oocyte maturation. Injection of the anti-XSSH antibody inhibited the assembly of cytoplasmic actin filaments at the basal (vegetal) region of nuclei before GVBD to suppress the formation of the MTOC-TMA, retained dense and globular actin filament clusters at the nuclear region after GVBD, and inhibited the formation of meiotic spindles. We previously reported that phalloidin injection prevented GVBD and the formation of MTOC-TMA at the basal part of the remaining nucleus (Okada et al., 2012). Here we provide more detailed data regarding the effects of phalloidin and jasplakinolide on the nuclear shrinkage and formation of microtubule structures. On the basis of past and present findings, we conclude that the assembly of the MTOC-TMA and meiotic spindles requires cytoplasmic and intranuclear actin filament reorganization regulated by XAC and XSSH during Xenopus oocyte maturation. In addition, because nocodazole treatment inhibited disassembly of intranuclear actin filaments from the vegetal side of nuclei, the MTOC-TMA could function as a regulator for disassembly of intranuclear actin filaments.

Figure 9 shows a model for the interplay between actin filaments and microtubule structures, in addition to their dynamics, during oocyte maturation. In stage VI oocytes, actin filament networks are well developed in the nuclei, which are surrounded by cytoplasmic actin filaments (Figure 9A). Under maturation, both cytoplasmic actin filaments and microtubules assemble to line up beneath the vegetal side of the nuclei immediately before GVBD (Figure 9B). These structures disappear, and the localization of the MTOC-TMA at the vegetal side of the nuclei is suppressed after the injection of either anti-XSSH antibody or phalloidin. Our results may indicate that XAC-mediated actin reorganization leads to the formation of the cytoplasmic actin filament bundles, where microtubules colocalize, at the vegetal side of nuclei. The de novo cytoplasmic actin filament assembly at the vegetal side of nuclei may be essential for the localization of the MTOC. The relocation of the components of the MTOC, including γ-tubulin, to the vegetal perinuclear cytoplasm has been reported to be dependent on cytoplasmic dynein and nuclear protein that associates with the mitotic apparatus (NuMA; Becker et al., 2003). Further studies are needed to examine whether these microtubule-dependent motor and microtubule–associated proteins coordinate with actin filaments to form the MTOC-TMA.

GVBD occurs initially at the vegetal side of nuclei and is accompanied by nuclear shrinkage, MTOC formation, and intranuclear actin filament disassembly beginning also from the vegetal side. The MTOC-TMA develops well, and the cytoplasmic actin filaments continue to be present at its base (Figure 9C). Our microinjection studies revealed that the nuclear shrinkage occurs independently of actin depolymerization. In addition, formation of the MTOC-TMA may induce the unidirectional disassembly of intranuclear actin filaments from the vegetal side, since a defect of MTOC-TMA formation, caused by anti-XSSH antibody or phalloidin injection or jasplakinolide or nocodazole treatment, suppresses disassembly of intranuclear actin filaments from the vegetal side of nuclei. The intranuclear actin filament disassembly progressing from the vegetal to the animal side might cause the development of the TMA and migration of the MTOC-TMA toward the animal pole. Note that the microtubules in the TMA did not enter the animal region, where the residual intranuclear actin filaments were still present (Figures 3C
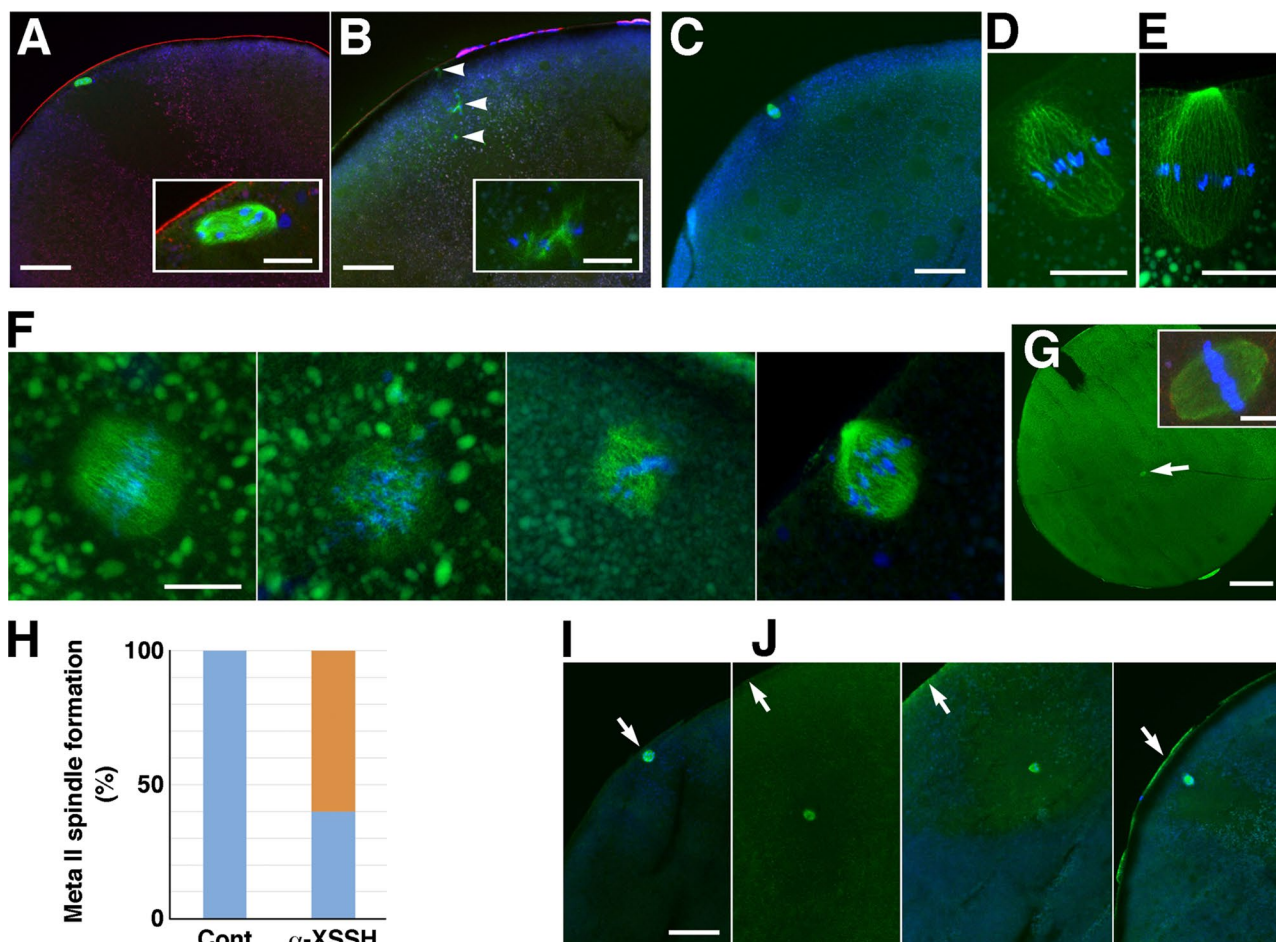
FIGURE 8: Effects of injection of anti-XSSH antibody (A–H) and S3A-cofilin (I, J) on assembly of meiotic spindles. Cryosections were triple stained with DAPI (blue), anti-microtubule antibody (green), and TMR-phalloidin (red; A, B, G inset) or double stained with DAPI (blue) and anti-microtubule antibody (green; C–G, I, J). (A) Control oocytes formed the metaphase I spindle (exactly prometaphase I) at the animal cortex (bar, 100 µm). The spindle is enlarged in the inset (bar, 20 µm). (B) Malformation of the metaphase I spindle is observed in the antibody-injected oocytes (bar, 100 µm). Arrowheads indicate disrupted microtubule bundles associated with chromosomes. Inset, enlarged image of one of the bundles (bar, 20 µm). (C–E) Representative images of metaphase II spindles oriented vertically to the cortex in the control oocytes. The spindle in C (bar, 100 µm) is enlarged in D (bar, 20 µm). Another example of metaphase II spindles is shown in E (bar, 20 µm). (F) Four examples of metaphase II spindles formed in the antibody-injected oocytes (bar, 20 µm). (G) An example of metaphase II spindles (arrow) formed at the center of the antibody-injected oocytes without anchoring to the cortex (bar, 200 µm). Inset, enlarged image of the spindle (bar, 20 µm). (H) Ratio of metaphase II spindles formed at the cortex (blue) to spindles formed at the center of oocytes (orange) in control ($n = 9$) and anti-XSSH antibody–injected oocytes ($n = 10$). (I, J) Metaphase I spindles formed at the cortex in a control oocyte (I) and formed in the yolk-free region without anchoring to the cortex in S3A-cofilin–injected oocytes (J; three examples are shown). Bar, 100 µm.

and 5B). When the residual intranuclear actin filaments disappear, the MTOC-TMA migrates to the animal side while maintaining the actin filaments at its base (Figures 3D and 9D). The specific factor(s) coordinating these actin filaments and microtubules have yet to be identified. In addition to myosin-X (Weber *et al.*, 2004), NabKin is an attractive candidate linking this process, since this protein binds to both actin filaments and microtubules and colocalizes with either intranuclear actin filaments or the MTOC-TMA (Samwer *et al.*, 2013). Formins may also be involved in cytoplasmic actin filament assembly at the vegetal side of nuclei, since they bind to microtubules in addition to nucleating actin filaments (Chesarone *et al.*, 2010; Gaillard *et al.*, 2011; Roth-Johnson *et al.*, 2014).

In this study, we also demonstrated that malformation of spindles is induced by injection of either anti-XSSH antibody or S3A-cofilin. Inhibition of XAC activation by antibody injection leads to stabilization of actin filaments, and S3A-cofilin may cause uncontrollable actin filament dynamics. These opposing effects on actin filament dynamics may both produce the malformation of spindles. Actin filaments have been previously reported to be associated with meiotic spindles in *Xenopus* oocytes (Weber *et al.*, 2004). Disruption of myosin X, which binds to both actin filaments and microtubules, causes the formation of actin aggregates and malformation of meiotic spindles, suggesting a direct functional link between actin filaments and spindle formation. Our results support this functional linkage and suggest a novel regulatory link between the actin filament dynamics and meiotic spindle formation during *Xenopus* oocyte maturation.
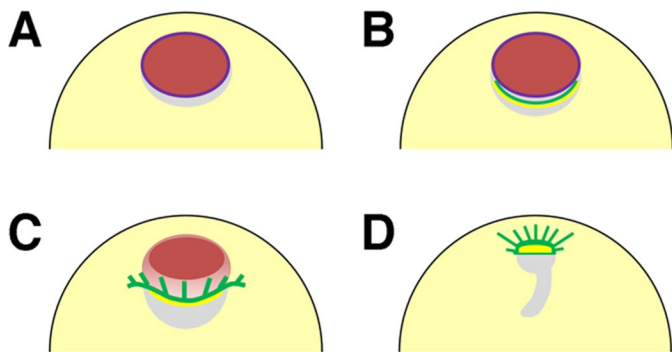
FIGURE 9: Summary of organization of microtubules and actin filaments during oocyte maturation in *Xenopus* oocytes. (A) Stage VI oocytes form dense intranuclear actin filament networks (red) and cytoplasmic actin filament bundles surrounding the nuclei (not shown). Purple line represents nuclear envelopes (lamin). (B) As maturation begins, microtubules and cytoplasmic actin filaments (green and yellow, respectively) concentrate to the perinuclear cytoplasm (yolk-free zone, gray) at the vegetal side of the nuclei in a process that is dependent on XAC-mediated actin dynamics; this process is inhibited by anti-XSSH antibody injection. (C) When GVBD occurs from the vegetal side of the nuclei, the nucleus begins to shrink, the MTOC-TMA (green) develops well, and the cytoplasmic actin filaments (yellow) remain at its base. The intranuclear actin filaments then begin to disassemble from the vegetal side of the nuclei (orange). Although the TMA elongates to the animal side, it never enters the animal region, where the residual intranuclear actin filaments (red) are still present. (D) Disassembly of intranuclear actin filaments leads to the migration of the MTOC-TMA to the animal side and subsequent formation of the first meiotic spindles. The gray region represents the yolk-free zone.

MATERIALS AND METHODS

Oocyte preparation and culture

Female *X. laevis* were anesthetized in ice water, and lobes of ovaries were excised from a small incision made in the posterior ventral side. Oocytes were obtained by manual defolliculation with watchmaker's forceps and maintained in OR2 medium (82.5 mM NaCl, 2.5 mM KCl, 1 mM CaCl$_2$, 1 mM MgCl$_2$, 1 mM Na$_2$HPO$_4$, 5 mM 4-(2-hydroxyethyl)-1-piperazineethanesulfonic acid [HEPES]–NaOH, pH 7.8) at 16°C in agarose-coated plastic dishes. For in vitro maturation, defolliculated stage VI oocytes were incubated in OR2 medium containing 5 µM progesterone at 19°C until GVBD, as indicated by the appearance of the WMS. Thereafter, oocytes were further incubated in OR2 medium at the indicated times. For the treatment of oocytes with jasplakinolide (Life Technologies, Osaka, Japan), defolliculated immature oocytes were incubated with 10 µM jasplakinolide or 0.1% dimethyl sulfoxide (DMSO; control) in OR2 medium for 3 h before progesterone addition. For the treatment of oocytes with nocodazole (purchased from Sigma-Aldrich, St. Louis, MO), progesterone-treated oocytes were incubated with 20 µg/ml nocodazole or 0.1% DMSO (control) at the relative time point of 0.5.

The timing of GVBD after progesterone exposure varied widely among oocytes. Therefore the progression of oocyte maturation until WMS formation was monitored based on relative time points; the addition of progesterone was designated as time point 0.0, and >80% oocytes with WMS formation was designated as time point 1.0. To obtain the oocytes that had just reached GVBD, the oocytes were collected under a dissection microscope immediately after WMS formation.

Sample preparation for SDS–PAGE

One oocyte was crushed by sonication in 20 µl of yolk-removing buffer (0.1 M NaCl, 2 mM ethylene glycol tetraacetic acid [EGTA], 1% Triton X-100, 0.05% SDS, 1 mM phenylmethylsulfonyl fluoride, and 20 mM NaPO$_4$ buffer, pH 7.0). After centrifugation at 13,000 rpm for 15 min, the supernatant was mixed with the same volume of SDS-sample buffer.

To monitor F-actin content in the nuclei, nuclei were manually isolated from maturing oocytes every hour after progesterone treatment until GVBD and placed into nuclei isolation buffer (140 mM KCl, 0.5 mM MgSO$_4$, 1 mM EGTA, 20 mM Tris-HCl, pH 7.5). Fifteen nuclei were crushed by pipetting in 20 µl of buffer containing 0.2% Tween 20 and immediately ultracentrifuged at 436,000 × *g* for 20 min at 4°C. The supernatants and pellets were dissolved in SDS-sample buffer, boiled for 5 min at 100°C and subjected to SDS–PAGE and immunoblotting.

For two-dimensional (2D) PAGE, >20 nuclei and several enucleated oocytes were homogenized by sonication directly in 150 µl SDS-sample buffer (4% SDS, 10% 2-mercaptethanol, 20% glycerol, and 50 mM Tris-HCl, pH 7.0) to avoid dephosphorylation of XAC. Proteins were precipitated by methanol/chloroform (Wessel and Flugge, 1984), dried, and dissolved in 2D PAGE buffer as described previously (Iwase *et al.*, 2013).

PAGE and immunoblotting

SDS–PAGE was carried out according to Laemmli (1970). The 2D PAGE was performed according to O'Farrell *et al.* (1977) using nonequilibrium-pH-gradient gel electrophoresis for the first dimension. For immunoblotting, proteins were electrophoretically transferred from the SDS gel to nitrocellulose membranes by the method of Towbin *et al.* (1979). The membranes were treated with 5% skimmed milk in PBS for 1 h and then incubated with antibodies as described previously (Iwase *et al.*, 2013). Quantification was carried out by densitometry with ImageJ (National Institutes of Health, Bethesda, MD).

Antibodies

Rabbit polyclonal anti-XSSH IgG for microinjection and immunofluorescence microscopy and guinea pig polyclonal anti-XSSH antibody for immunoblotting were prepared as described previously (Tanaka *et al.*, 2005b; Iwase *et al.*, 2013). For microinjection, purified rabbit anti-XSSH IgG was conjugated with an NLS-peptide (CAPK-KKRKV) as follows. IgG (750 µl) dissolved in 50 mM NaCl and 0.1 M NaPO$_4$ buffer (pH 7.0) was incubated with 75 µl of 5 mg/ml 4-maleimidobutyric acid *N*-hydroxysuccinimide ester in DMSO at room temperature for 1 h. The sample was gel-filtrated by PD-10 column (GE Healthcare, Piscataway, NJ) preequilibrated with 50 mM NaCl, 10 mM MgCl$_2$, and 10 mM NaPO$_4$ buffer (pH 6.3). IgG fraction (1 ml) was incubated with 400 µl of 1 mM NLS-peptide dissolved in 10 mM MgCl$_2$, 5 mM EDTA, and 0.1 M NaPO$_4$ buffer (pH 7.0) at 30°C for 30 min. Then dithiothreitol was added to the mixture and incubated for 1 h. NLS-peptide–conjugated IgG (anti-XSSH IgG-NLS) was precipitated with 50% saturation of ammonium sulfate, centrifuged, and dialyzed to the injection buffer (60 mM KCl, 2 mM MgCl$_2$, and 5 mM HEPES-KOH, pH 7.2) at a final concentration of 10 mg/ml. For injection control, the monoclonal antibody specific for avian and mammalian cofilin (MAB-22) was used, since this antibody does not bind to XAC. MAB-22 IgG was purified using protein G–Sepharose (GE Healthcare) from the mouse ascites fluid produced by injecting the MAB-22 hybridomas and injected at a concentration of 10 mg/ml. MAB-22 IgG conjugated with an NLS-peptide as described was also used for injection control.

Anti-XAC monoclonal and polyclonal antibodies were previously prepared (Okada *et al.*, 1999). Anti-XCap1 polyclonal antibody was raised in rabbits by injecting purified full-length XCap1 expressed in *Escherichia coli*. Anti-actin polyclonal antibody and anti–*Xenopus* lamin III antibody were kindly provided by K. Iida (Tokyo Metropolitan Institute of Medical Science, Tokyo, Japan; Iida and Yahara, 1986) and K. Ohsumi (Nagoya University, Nagoya, Japan), respectively. Monoclonal antibodies against tubulin (DM1A) and coilin (H1) were purchased from Sigma-Aldrich and Santa Cruz Biotechnology (Shanghai, China), respectively. Coilin is a component of nuclear pearls, novel Cajal body–like structures in the *Xenopus* GV (Nizami and Gall, 2012). Alexa 488–labeled goat anti-mouse or rabbit IgG or TMR-labeled goat anti-mouse or rabbit IgG were purchased from Invitrogen (San Diego, CA). Alkaline phosphatase–conjugated goat anti-mouse, rabbit, and guinea pig IgG were purchased from Bio-Rad Laboratories (Hercules, CA) and Chemicon (Temecula, CA). TMR- or Alexa 488–conjugated phalloidin was purchased from Invitrogen.

Microinjection into oocytes
A 1:1 mixture of anti-XSSH IgG and anti-XSSH IgG-NLS and constitutively active S3A chick cofilin (Nagaoka *et al.*, 1996) were used for injection. Injection volumes from a pressure injector (CIJ-1; Shimadzu, Kyoto, Japan) were calibrated by measuring the volume of an aqueous drop delivered into mineral oil. Injections were given in OR2 medium containing 5% Ficoll PM400 (GE Healthcare) by inserting a glass needle into the marginal zone of an oocyte in a volume of 20–30 nl/oocyte. After injection, the injected oocytes were incubated in OR2 medium for at least 2 h at 16°C and then treated with progesterone to induce oocyte maturation at 19°C. Phalloidin injection was carried out as described elsewhere (Okada *et al.*, 2012).

Isolation of oocyte nuclei for immunofluorescence microscopy
Defolliculated oocytes were placed on a piece of parafilm to remove the residual OR2 medium transferred into mineral oil. The nuclei were isolated manually with forceps and immediately transferred into anhydrous acetone precooled at −30°C and incubated at the same temperature for 2 d. The nuclei were fixed and rehydrated according to the methods of Bohnsack *et al.* (2006) and double stained with Alexa 488–phalloidin and anti-lamin antibody as described later.

Immunofluorescence microscopy
It is important to note that the fixation of oocytes with formaldehyde at room temperature is not suitable for preserving the intranuclear actin filament structure and subcellular localization of XAC, at least in *Xenopus*. The intranuclear actin filament networks can be observed when oocytes have been quickly frozen (Bohnsack *et al.*, 2006). Moreover, XAC seemed to colocalize with the MTOC-TMA and spindles when observed in paraffin-embedded sections of formaldehyde-fixed oocytes by immunofluorescence microscopy (unpublished data). The cytoplasmic-soluble proteins might nonspecifically bind to microtubule structures during the duration of the formaldehyde fixation step at room temperature. Therefore, in this study, oocytes were quick-frozen, fixed, and cut into 35-μm-thick cryosections according to the methods of Bohnsack *et al.* (2006). Sections were incubated with primary antibodies or fluorescent phalloidin for 3–16 h at 4°C and then with fluorophore-conjugated secondary antibodies for 2 h at 4°C. For XAC or XSSH staining, sections were postfixed with 99.5% ethanol at room temperature for 15 min before incubation with primary antibodies. After each immunoreaction step, the sections were rinsed and washed with PBS. The sections were mounted in PBS containing 1 mg/ml *p*-phenylenediamine and 90% glycerol. Confocal images were acquired with an Olympus FV1000.

REFERENCES
Abe H, Obinata T, Minamide LS, Bamburg JR (1996). *Xenopus laevis* actin-depolymerizing factor/cofilin: a phosphorylation-regulated protein essential for development. J Cell Biol 132, 871–885.

Abe H, Oshima S, Obinata T (1989). A cofilin-like protein is involved in the regulation of actin assembly in developing skeletal muscle. J Biochem 106, 696–702.

Almonacid M, Terret ME, Verlhac MH (2014). Actin-based spindle positioning: new insights from female gametes. J Cell Sci 127, 477–483.

Arber S, Barbayannis FA, Hanser H, Schneider C, Stanyon CA, Bernard O, Caroni P (1998). Regulation of actin dynamics through phosphorylation of cofilin by LIM-kinase. Nature 393, 805–809.

Becker BE, Romney SJ, Gard DL (2003). XMAP215, XKCM1, NuMA, and cytoplasmic dynein are required for the assembly and organization of the transient microtubule array during the maturation of *Xenopus* oocytes. Dev Biol 261, 488–505.

Bernstein BW, Bamburg JR (2010). ADF/cofilin: a functional node in cell biology. Trends Cell Biol 20, 187–195.

Bohnsack MT, Stüven T, Kuhn C, Cordes VC, Görlich DA (2006). Selective block of nuclear actin export stabilizes the giant nuclei of *Xenopus* oocytes. Nat Cell Biol 8, 257–263.

Chesarone MA, DuPage AG, Goode BL (2010). Unleashing formins to remodel the actin and microtubule cytoskeletons. Nat Rev Mol Cell Biol 11, 62–74.

Field CM, Lénárt P (2011). Bulk cytoplasmic actin and its functions in meiosis and mitosis. Curr Biol 21, 825–830.

Gaillard J, Ramabhadran V, Neumanne E, Gurel P, Blanchoin L, Vantard M, Higgs HN (2011). Differential interactions of the formins INF2, mDia 1, and mDia 2 with microtubules. Mol Biol Cell 22, 4575–4587.

Gard DL (1992). Microtubule organization during maturation of *Xenopus* oocytes: assembly and rotation of the meiotic spindles. Dev Biol 151, 516–530.

Gard DL, Cha BJ, Roeder AD (1995). F-actin is required for spindle anchoring and rotation in *Xenopus* oocytes: a re-examination of the effects of cytochalasin B on oocyte maturation. Zygote 3, 17–26.

Iida K, Yahara I (1986). Reversible induction of actin rods in mouse C3H-2K cells by incubation in salt buffers and by treatment with non-ionic detergents. Exp Cell Res 164, 492–506.

Iwase S, Sato R, De Bock PJ, Gevaert K, Fujiki S, Tawada T, Kuchitsu M, Yamagishi Y, Ono S, Abe H (2013). Activation of ADF/cofilin by phosphorylation-regulated Slingshot phosphatase is required for the meiotic spindle assembly in *Xenopus laevis* oocytes. Mol Biol Cell 24, 1933–1946.

Jessus C, Huchon D, Ozon R (1986). Distribution of microtubules during the breakdown of the nuclear envelope of the *Xenopus* oocyte: an immunocytochemical study. Biol Cell 56, 113–120.

Laemmli UK (1970). Cleavage of structural proteins during the assembly of the head of bacteriophage T4. Nature 227, 680–685.

Li R, Albertini DF (2013). The road to maturation: somatic cell interaction and self-organization of the mammalian oocyte. Nat Rev Mol Cell Biol 14, 141–152.

Loeder AD, Gard DL (1994). Confocal microscopy of F-actin distribution in Xenopus oocytes. Zygote 2, 111–124.

Masui Y, Clarke HJ (1979). Oocyte maturation. Int Rev Cytol 57, 185–282.

Nagaoka R, Abe H, Obinata T (1996). Site-directed mutagenesis of the phosphorylation site of cofilin: its role in cofilin-actin interaction and cytoplasmic localization. Cell Motil Cytoskeleton 35, 200–209.

Nagata-Ohashi K, Ohta Y, Goto K, Chiba S, Mori R, Nishita M, Ohashi K, Kousaka K, Iwamatsu A, Niwa R, Uemura T, Mizuno K (2004). A pathway of neuregulin-induced activation of cofilin-phosphatase Slingshot and cofilin in lamellipodia. J Cell Biol 165, 465–471.

Niwa R, Nagata-Ohashi K, Takeichi M, Mizuno K, Uemura T (2002). Control of actin reorganization by Slingshot, a family of phosphatases that dephosphorylate ADF/cofilin. Cell 108, 233–246.

Nizami ZF, Gall JG (2012). Pearls are novel Cajal body-like structures in the *Xenopus* germinal vesicle that are dependent on RNA pol III transcription. Chromosome Res 20, 953–969.

O'Farrell PG, Goodman HM, O'Farrell PH (1977). High resolution two-dimensional electrophoresis of basic as well as acidic proteins. Cell 12, 1133–1141.

Okada I, Fujiki S, Iwase S, Abe H (2012). Stabilization of actin filaments prevents germinal vesicle breakdown and affects microtubule organization in *Xenopus* oocytes. Cytoskeleton 69, 312–323.

Okada K, Obinata T, Abe H (1999). XAIP1: a *Xenopus* homologue of yeast actin interacting protein 1 (AIP1), which induces disassembly of actin filaments cooperatively with ADF/cofilin family proteins. J Cell Sci 112, 1553–1565.

Ono S (2007). Mechanism of depolymerization and severing of actin filaments and its significance in cytoskeletal dynamics. Int Rev Cytol 258, 1–82.

Roth-Johnson EA, Vizcarra CL, Bois JS, Quinlan ME (2014). Interaction between microtubules and the Drosophila formin Cappuccino and its effect on actin assembly. J Biol Chem 289, 4395–4404.

Samwer M, Dehne HJ, Spira F, Kollmar M, Gerlich DW, Urlaub H, Gorlich D (2013). The nuclear F-actin interactome of *Xenopus* oocytes reveals an actin-bundling kinesin that is essential for meiotic cytokinesis. EMBO J 32, 1886–1902.

Sandquist JC, Kita AM, Bement WM (2011). And the dead shall rise: actin and myosin return to the spindle. Dev Cell 21, 410–419.

Soosairajah J, Maiti S, Wiggan O, Sarmiere P, Moussi N, Sarcevic B, Sampath R, Bamburg JR, Bernard O (2005). Interplay between components of a novel LIM kinase-slingshot phosphatase complex regulates cofilin. EMBO J 24, 473–486.

Takahashi T, Koshimizu U, Abe H, Obinata T, Nakamura T (2001). Functional involvement of *Xenopus* LIM kinases in progression of oocyte maturation. Dev Biol 229, 554–567.

Tanaka K, Nishio R, Haneda K, Abe H (2005a). Functional involvement of *Xenopus* homologue of ADF/cofilin phosphatase, Slingshot (XSSH), in the gastrulation movement. Zool Sci 22, 955–969.

Tanaka K, Okubo Y, Abe H (2005b). Involvement of slingshot in the Rho-mediated dephosphorylation of ADF/cofilin during *Xenopus* cleavage. Zool Sci 22, 971–984.

Towbin H, Staehelin T, Gordon J (1979). Electrophoretic transfer of proteins from polyacrylamide gels to nitrocellulose sheets: procedure and some applications. Proc Natl Acad Sci USA 76, 4350–4354.

Van Troys MV, Huyck L, Leyman S, Dhaese S, Vandekerkhove J, Ampe C (2008). Ins and outs of ADF/cofilin activity and regulation. Eur J Cell Biol 87, 649–667.

Weber KL, Sokac AM, Berg JS, Cheney RE, Bement WM (2004). A microtubule-binding myosin required for nuclear anchoring and spindle assembly. Nature 431, 325–329.

Wessel D, Flugge UI (1984). A method for the quantitative recovery of protein in dilute solution in the presence of detergents and lipids. Anal Biochem 138, 141–143.

Yang N, Higuchi O, Ohashi K, Nagata K, Wada A, Kangawa K, Nishida E, Mizuno K (1998). Cofilin phosphorylation by LIM-kinase 1 and its role in Rac-mediated actin reorganization. Nature 393, 809–812.

Yi K, Li R (2012). Actin cytoskeleton in cell polarity and asymmetric division during mouse oocyte maturation. Cytoskeleton 69, 727–737.